In-Depth Study of Chemically Electrodeposited Cuprous Oxide (Cu2O) thin Films on ITO Glass

Fatima Zohra Nouasria, Djamel Selloum, Omar Ben Elkhettab Mokrani, Fares Fenniche, Sophie Tingry, Yasmina Khane, Abdellah Henni, Hakim Belkhalfa, Nadir Dizge, Salim Albukhaty, et al.

Plasmonics, 2024, in press.

In-depth study of chemically electrodeposited cuprous oxide (Cu_2O) thin films on ITO glass

Fatima Zohra Nouasria [a*], Djamel Selloum [b], Omar Ben Elkhettab Mokrani [a], Fares Fenniche [c,d], Sophie Tingry [e], Yasmina Khane [d,f], Abdellah Henni [g], Hakim Belkhalfa [h], Nadir Dizge [i], Salim Albukhaty[j]*, Ghassan M. Sulaiman[k].

[a] *Process Engineering Laboratory (PEL), Kasdi Merbah University, Ouargla, 30000, Algeria*

[b] *Laboratoire Croissance et Caractérisation de Nouveaux Semi-conducteurs, Université Ferhat Abbas, Sétif-1, 19000, Algeria*

[c] *Department of Process Engineering, Faculty of Sciences and Technology, University of Ghardaïa, BP 455, 47000 Ghardaïa– Algeria*

[d] *Materials, Energy Systems Technology and Environment Laboratory, Faculty of Sciences and Technology, University of Ghardaïa, BP 455, 47000 Ghardaïa, Algeria*

[e] *Institut Européen des Membranes, UMR 5635, Université Montpellier, ENSCM, CNRS, Montpellier, France*

[f] *Faculty of Sciences and Technology, University of Ghardaïa, BP 455, 47000 Ghardaïa, Algeria*

[g] *Dynamic Interactions and Reactivity of Systems Laboratory, Kasdi Merbah University, Ouargla, 30000, Algeria*

[h] *Scientific and Technical Research Center in Physicochemical Analysis, Bou-Ismail, Tipaza, Algeria*

[I] *Department of Environmental Engineering, Mersin University, Mersin, 33343, Turkey*

j Department of Chemistry, College of Science, University of Misan, Maysan 62001, Iraq.

k Division of Biotechnology, Department of Applied Science, University of Technology, Baghdad, 10066, Iraq.

Correspondence : nouasria.fatimazohra@gmail.com ; albukhaty.salim@uomisan.edu.iq

Abstract

In this contribution, we report the screening of different parameters contributing to the electrodeposition of Cu_2O nanostructures as an electrode material to provide an overall understanding of the effect of the entire method conditions. We varied different parameters (pH, potential, and deposition time) during the electrodeposition of cuprous oxide (Cu_2O) thin films on ITO glass substrate and integrated different methods: X-ray diffraction (XRD), UV-vis absorption (UV-Vis), scanning electron microscope (SEM), cyclic voltammetry (CV), and chronoamperometry (CA) to deeply examine the as-synthesized materials and interrogate their efficiency towards the conversion of light to current (photo-current). From the chronoamperometry experiments, all the curves of current transients exhibit a typical response of a progressive 3D nucleation growth. Highly crystalline Cu_2O structures of nano-cubes can be seen in the XRD and SEM results at high pH (12.5) and at potentials -0.5 and -0.6 V Vs. SCE during 60 min of deposition time. UV-Vis results showed high optical absorption in the region of 300-500 nm. The photocurrent measurements of Cu_2O coupled with Cu-doped ZnO suggested that the synthesized Cu_2O proved to be the best candidate as a solar cell.

Keywords: electrodeposition, Cu_2O, pH, potential, deposition time, ZnO, thin film.

1. Introduction

The development of new, more efficient, and less expensive solar converters requires new approaches that focus on low-cost, non-toxic materials produced using energy-efficient processes. Cuprous oxide (Cu_2O) thin films are considered an active component in solar cells, allowing them to form junctions with other oxidized semiconductors such as TiO_2 and ZnO [1,2]. Synthesis of cuprous oxide (Cu_2O) thin films has attracted greater attention for many reasons, and besides the various properties which are known with it, (i) a direct bandgap of about 2 eV at room temperature (around 25 °C). The origin of p-type conductivity in Cu_2O (ii) the intrinsic defects present in the

material such as copper vacancies that form an acceptor level, (iii) the absorption coefficient in a wide range of wavelengths of the solar spectrum, (iv) chemical stability, (v) nontoxicity, (vi) high hole-mobility at room temperature, and (vii) low cost and availability of elements in the earth's crust [3,4].

Compared to vacuum-based methods, electrochemical deposition is a simple and cost-effective technique for growing thin films, as it affords close control of reactions during the deposition process and control of growth and structure, which in turn allows for monitoring of the deposition materials and provides many opportunities for material modification [5,6]. As a result, this method has received considerable attention for the deposition of metals and semiconductor materials [7–9]. The electrodeposition of p-type Cu_2O thin films is usually performed in a basic electrolyte containing Cu^{2+} ions and a chelating agent such as f lactic acid, citric acid, or tartaric acid to prevent Cu precipitation in basic conditions [10].

Changing the electrodeposition parameters has a great influence on the Cu_2O thin film deposition, resulting in various final morphologies and properties. Extensive literature is available regarding the influence of the pH of the solution [11–14] the applied potential [15–17] and the deposition time [18–21] on the energy conversion efficiencies of solar cells. However, the results are difficult to compare because the works dealing with the effect of all the reaction parameters related to the Cu_2O thin film deposition are rarely available.

To this end, this work was motivated by the desire to study in-depth the effect of the electrodeposition conditions, and thus presents a systematic investigation aiming to establish the influence of the pH of the solution, applied potential, and deposition time on the kinetics parameters, structural, morphological, and optical properties of the electrodeposited Cu_2O thin films for further applications based on Cu_2O heterojunction solar cells.

2. Materials and characterization

Materials

The indium-doped tin oxide (ITO, resistivity ~ 30 ohm/square) glass (SOLEMS) was cut with the size 1 cm × 3 cm. $CuSO_4.5\ H_2O$ (purity ≥ 98%), $C_6H_8O_7$ (purity ≥ 99.5%), and NaOH (purity ≥ 98%) were purchased from Sigma Aldrich and used as received. All solutions were prepared with double distilled water.

Synthesis of Cu_2O thin films

The cuprous oxide (Cu_2O) thin films electrodeposition was carried out with a standard three-electrode cell system connected to an Autolab (PGSTAT 204) potentiostat/galvanostat and NOVA.1 software. The reference electrode

was a saturated calomel electrode (SCE), the counter electrode was a platinum electrode, and an ITO glass substrate was used as the working electrode (1cm^2). The ITO electrode was previously ultrasonically cleaned in solutions of acetone, ethanol, and distilled water. The electrodeposition process was performed in solutions containing 0.05 M $CuSO_4$ and 0.05 M $C_6H_8O_7$ as chelating agents at 65 °C. The pH of the solution was adjusted with NaOH to get the desired value.

Characterization techniques

The physicochemical characterizations of the synthesized materials were performed by scanning electron microscope (JEOL JSM-7001F) to capture the surface morphology of the films, XRD analysis to identify the crystallite structure (Bruker AXS D8 Advance Cu- Kα radiation, λ = 1.54 Å). The optical transmittance data of the films were obtained using a spectrophotometer (UV-2300, Shimadzu). The cyclic voltammetry measurements were conducted at 65 °C between +0.5 and -1.2 V vs. SCE and at the scan rate of 20 mVs^{-1}. chronoamperometry analysis was performed to determine the nucleation and the growth mechanism. The photocurrent response of the prepared materials was measured in 0.1 M Na_2SO_4 with the Autolab (PGSTAT 204) potentiostat/galvanostat and NOVA.1 software.

3. Results and discussion

3.1 Effect of the pH of the solution on Cu_2O electrodeposition

As a starting point, the influence of the pH of the solution was studied to optimize Cu_2O deposition. To this end, the two values pH=9 and 12.5 were tested (. Figure 1 shows the electrochemical behavior of the substrate (ITO) in the presence of Cu(II) ions, supporting electrolyte and NaOH (4 M) to adjust the pH value. As one can see from the forward scan, a reduction peak starting at -0.4 V vs. SCE is shown which was attributed to the reduction of Cu^{2+} to Cu^{+} (Reaction 1). The generated Cu^{+} ions then react with hydroxide ions to form $Cu(OH)_2$ which is transformed by dehydration into Cu_2O on the ITO surface (Reaction 2) [22,23]. The second reduction peak at about -0.8 V is ascribed to the deposition of metallic Cu (Reaction 3), Then, the cathodic current was increased which is related to the evolution of hydrogen reaction.

On the reverse scan, the shoulder observed at 0 V vs. SCE is attributed to the oxidation of Cu_2O to CuO and Cu^{2+} ions [24–26], while the intense peak at +0.3 V vs. SCE corresponds to the redissolution of Cu to Cu^{2+}.

$$Cu^{2+} + e^{-} \rightarrow Cu^{+} \qquad 1$$

$$2Cu^{+} + 2OH^{-} \rightarrow 2CuOH \rightarrow Cu_2O + H_2O \quad (2)$$

$$Cu^{2+} + 2e^{-} \rightarrow Cu \quad (3)$$

The peak appearance at +0.3 V vs. SCE confirms the formation of Cu_2O from the reduction of Cu^{2+} to Cu^{+} at the beginning of the forward sweep, as reported above. The presence of an intersection between the cathodic and anodic currents is characteristic of the formation of a new phase on the electrode [27]. The shapes of the voltammograms are consistent with those previously reported in the literature [23,28,29].

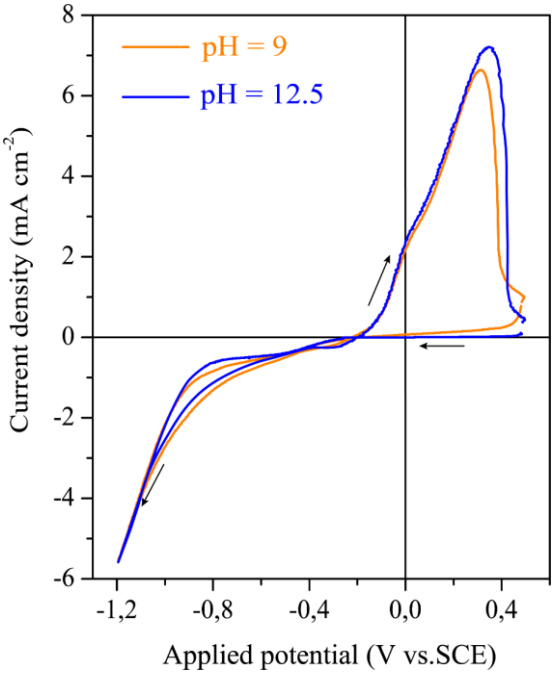

Figure 1: Cyclic voltammograms of Cu_2O electrodeposited on ITO glass substrate at pH 9 and pH 12.5, at 20 mVs^{-1} (in 0.05 M $CuSO_4$ + 0.05 M $C_6H_8O_7$ + 1 M NaOH solution) at 65°C

As shown in Figure 1, the current increases slightly by 10% for the deposition bath at pH 12.5, indicating a faster rate of Cu_2O deposition. Based on these results, the deposition potential of -0.5 V vs. SCE was selected to ensure the electrodeposition of Cu_2O while avoiding Cu formation.

3.1.1 Chronoamperometry analysis

Chronoamperometry experiments were thereafter carried out in order to determine the following kinetic parameters: the diffusion coefficient of Cu^{2+} ions in the electrolyte and the nucleation rate of Cu_2O. Figure 2a shows the following steps during chronoamperometry (E = -0.5 V vs. SCE): a high current density from the first seconds of the experiment corresponding to the charging of the double layer at the ITO/electrolyte interface,

followed by a decrease of the cathodic current as the surface is covered with a Cu_2O film (nucleation and growth of Cu_2O nuclei), and finally the value of the cathodic current density stabilizes as the deposition time increases due to the growth process of the Cu_2O film on the ITO substrate. Figure 2b clearly shows that all the transient curves exhibit a typical response curve of a progressive 3D nucleation growth [30,31].

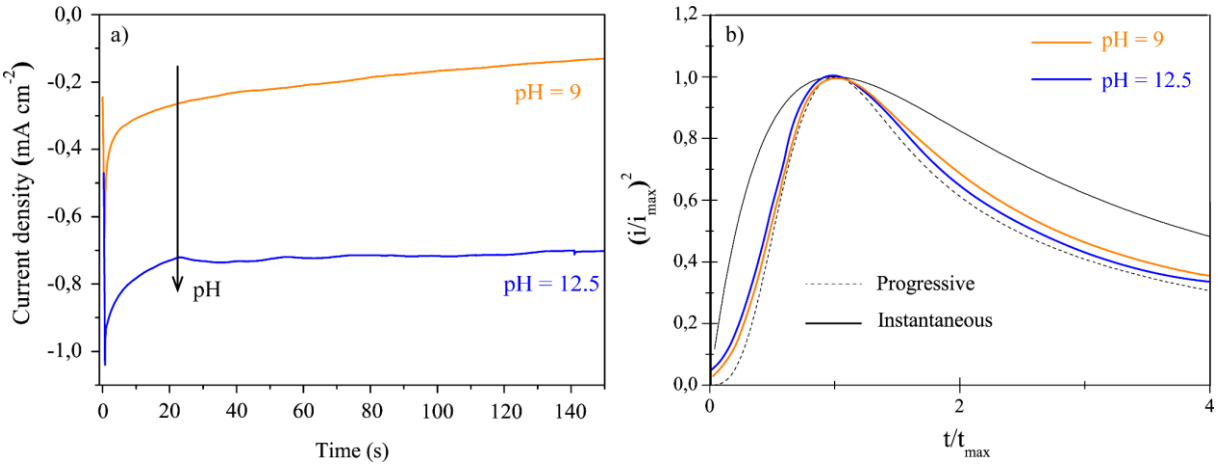

Figure 2: a) Experimental current transient curves. **b)** Non-dimensional $((i/i_{max})^2$ vs. $t/t_{max})$ plots at different bath pH.

The diffusion coefficient (D_{prog}) and the nucleation rate (AN_0) as a function of the pH were calculated from Equations 4 and 5 and summarized in Table 1.

$$i_{max}^2 t_{max} = 0.2598(zFC)^2 D_{prog} \quad (4)$$

$$AN_0 = 0.2898(8\pi CM/\rho)^{-1/2} zFC^2 i_{max}^2 t_{max}^3 \quad (5)$$

Where D is the diffusion coefficient, z is the number of transferred electrons per ion which is equal to 2, M is the atomic weight, t is time, F is the Faraday constant (96500 $C.mol^{-1}$), C is the bulk concentration of the electroactive species, and ρ is the density.

Table 1: Kinetic parameters extracted from the current transient for Cu_2O deposited at different pH.

pH	**AN_0 ($cm^{-2}. s^{-1}$)**	**D_{prog} ($cm^2.s^{-1}$)**
9	$1.37\times10^{+5}$	4.6×10^{-8}
12.5	$4.06\times10^{+5}$	1.2×10^{-7}

The results show that the diffusion coefficient of Cu^{2+} ions in the electrolyte increases from 4.6×10^{-8} to 1.2×10^{-7} $cm^2.s^{-1}$ when the pH increases from 9 to 12.5. In addition, the nucleation rate increases to reach a maximum value ($4.06 \times 10^{+5}$. cm^{-2}. s^{-1}) for pH 2.5. This can be explained by the fact that higher pH results in the release of more OH^- ions [32], which gives Cu^+ and OH^- ions more chances to react and leads to a larger amount of Cu_2O deposited on the ITO glass substrate.

3.1.2 Structural characterization

To evaluate the influence of the pH on the Cu_2O electrodeposition, we characterized the electrodeposited Cu_2O nanostructures by XRD. Figure 3 shows that the resulting materials exhibit 5 narrow and sharp peaks at 2θ values of 29.56°, 36.47°, 42.40°, 61.39°, and 73.57°, corresponding to (110), (111), (200), (220), and (311) planes, respectively, thus confirming the successful synthesis of a cubic phase crystal form of Cu_2O which is in perfect agreement with JCPDS card No 01-078-2076 [33,34]. No corresponding peak to copper oxide or metallic copper peak is observed.

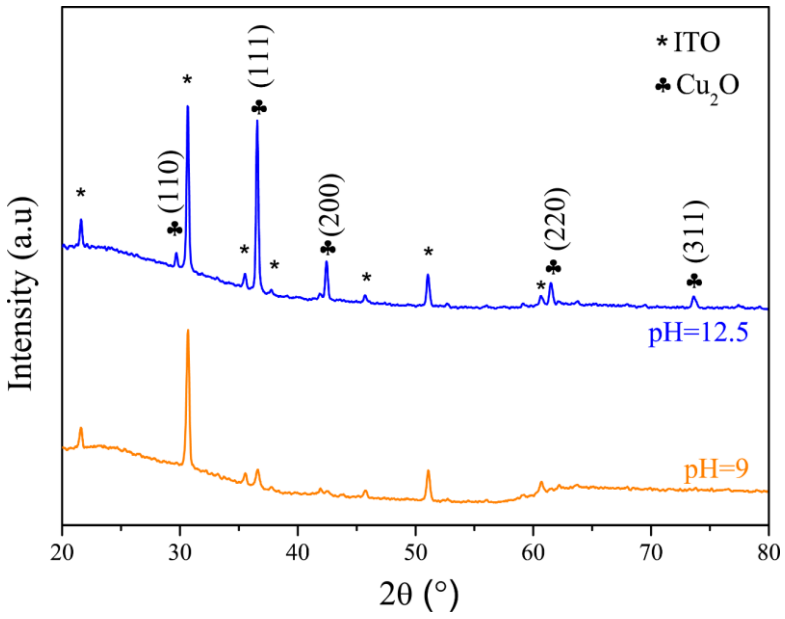

Figure 3: XRD patterns of Cu_2O nanostructures deposited at different pH values. (*) For ITO diffraction peaks.

The high intensity of the diffraction peak (111) at pH 9, shows that Cu_2O preferentially develops in this direction. Moreover, the intensity of the diffraction peaks (111) increases with the increase in the pH of the bath. Such observations were also reported in some previous studies [35–37]. The pH strongly affects the preferential orientation of Cu_2O nanostructures. The density of oxygen atoms per unit area differs for Cu_2O planes (100), (110),

and (111), with values of 2.78, 5.89, and 8.83 nm^{-2}, respectively. Consequently, under low pH conditions, the (100) direction is favored due to its lower oxygen atom density, while under high pH conditions, growth primarily occurs along the (111) direction, which has the highest density of oxygen atoms [38]. Since OH^- ions are a source of oxygen, the pH determines the preferential orientation and growth rate of crystalline. At pH 12.5, the adsorption of OH^- ions accelerate and therefore more O atoms are available and it becomes easier for deposition to occur on the (111) faces compared to those on (100) or (110) [39].

As shown in Table 2, the average crystallite size calculated from (111) peak for pH values 9 and 12.5 are 8.8 and 31.2 nm, respectively, and confirm the increase of the grain size with higher basic pH. The same, Zhou et al. [40] obtained an increase in the grain size of Cu_2O when the pH changes from 8 to 12. They attributed this change to the variation in the deposition rate at different pH.

Table 2: The average crystallite size of Cu_2O estimated at the diffraction peak (111) for various pH of the bath solution.

pH	2θ (°)	D (nm)
9	36.5	8.8
12.5	36.5	31.2

3.1.3 Morphological characterization

To gain further insights into the morphology, SEM analysis was undertaken for the Cu_2O thin films electrodeposited on ITO at different pH. Figure 4 points out the significant impact of pH on the grain size of the films. A triangular prism morphology covers the surfaces uniformly. As the pH of the solution increases, the three-faced pyramid becomes larger with sharp edges and corners due to the reduced nucleation density. The crystal surface with the slowest growth rate mainly controls the surface morphology during crystal growth. Therefore, as the pH increases, the concentration of OH^- increases and promotes the formation of the plane (111) [41]. Our findings fit well with the XRD results and with previously reported observations [37,42,43]. These results indicate that the pH of the solution has a major effect on the surface morphology of electrodeposited Cu_2O films.

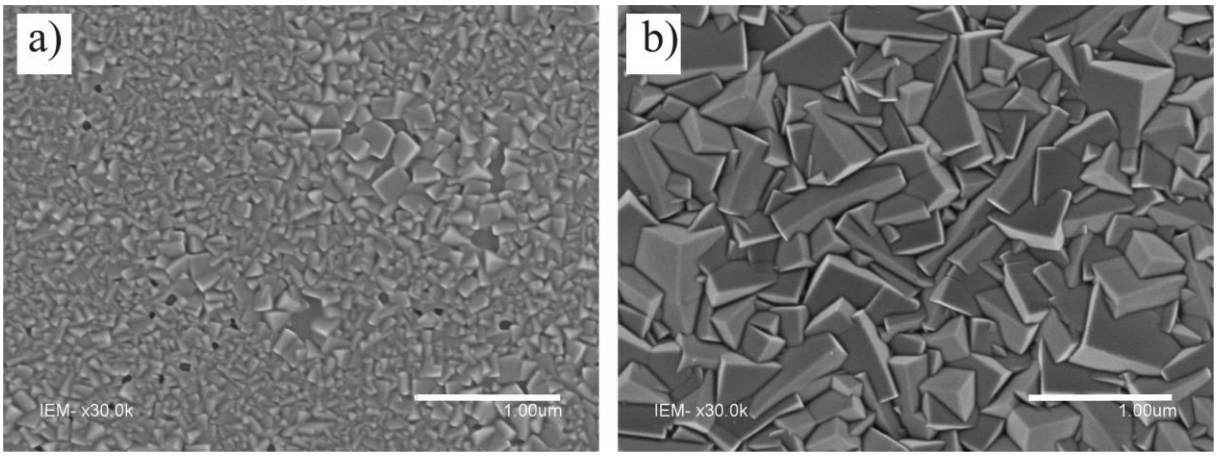

Figure 4: SEM images for Cu_2O films with different pH values: **a)** pH = 9 and **b)** pH = 12.5.

3.1.4 Optical characterization

The optical characteristic of Cu_2O nanostructures obtained at pH 9 and 12.5 was studied by UV-visible spectrophotometer with the ITO glass used as reference.

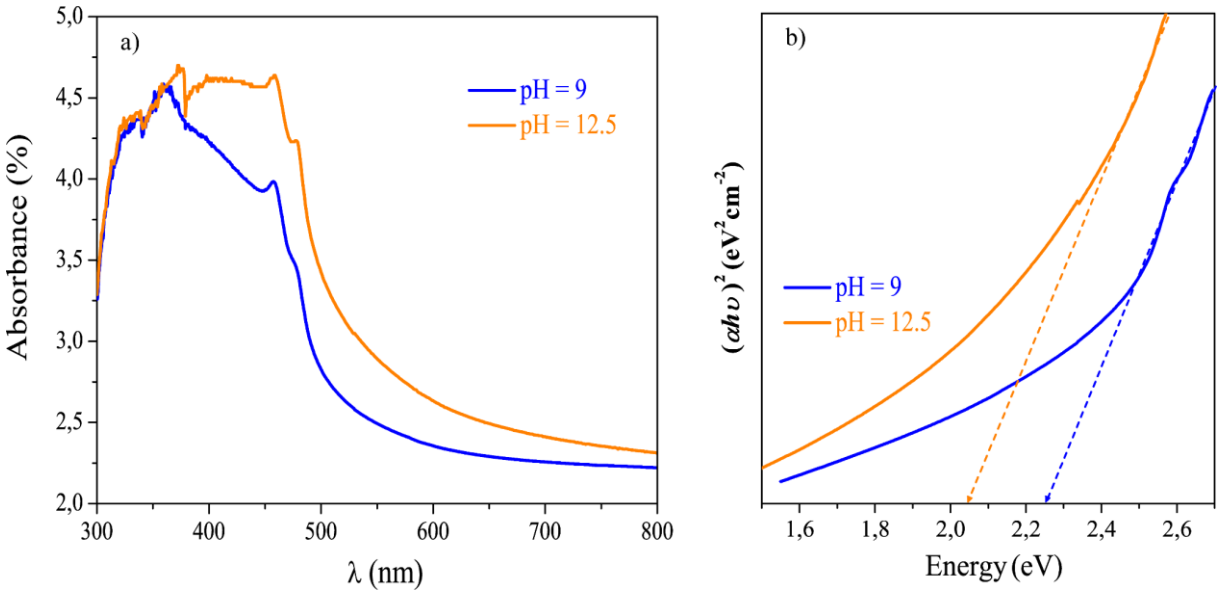

Figure 5: a) Absorption spectra of Cu_2O obtained at different pH solutions. **b)** Tauc plots for Cu_2O thin film.

The spectra in Figure 5a show high optical absorption in the region 300-500 nm with an increased absorption for pH 12.5. The absorption edge has a red shift and as the pH increases the visible absorption increases. The values of the gap energy (Eg), estimated from the Tauc plots (Figure 5. b), were 2.33 and 2.04 eV for pH 9 and 12.5, respectively. This decrease in the bandgap is due to the increase in the film thickness and crystallite size [44].

These observations match well with previous research on the development of Cu_2O nanostructures in different pH baths [36,44–46].

3.2 Effect of the applied potential on Cu_2O electrodeposition

3.2.1 Chronoamperometry analysis

In order to study in detail, the mechanism of the Cu_2O electrodeposition on the ITO substrate, a series of current transients (i-t) curves at different values of applied potential: -0.4, -0.5 and, -0.6 V vs. SCE were recorded. As shown in Figure 6a, the current density increases proportionally as the deposition potential tends to have more negative values, which is related to the increase in the deposition rate and density of Cu_2O [31]. From Figure 6b, it is clear that all the transients exhibit a typical response curve of a progressive (3D) nucleation-growth electrochemical process [47–49].

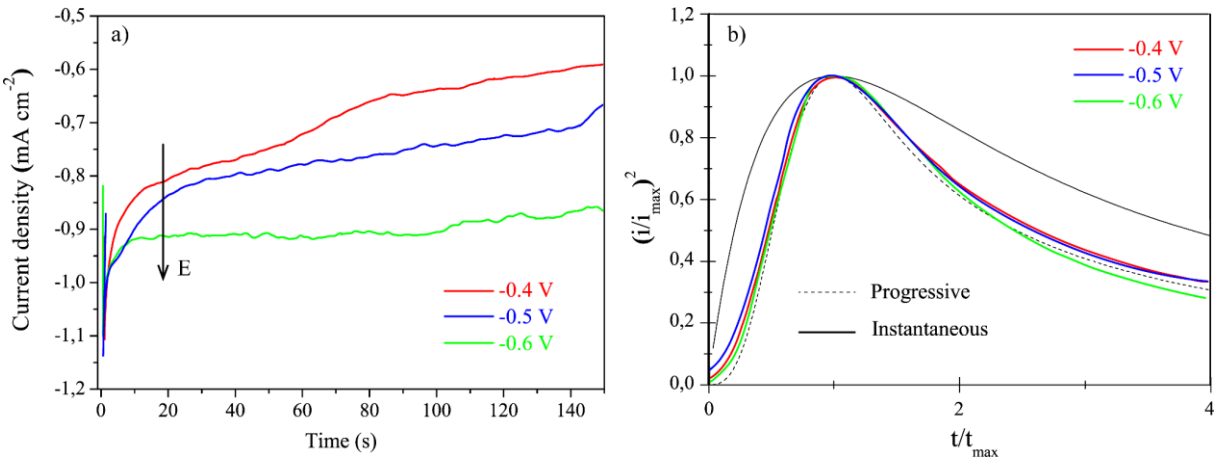

Figure 6: a) Experimental current transient. **b)** Non-dimensional $((i/i_{max})^2$ vs. $t/t_{max})$ plots at different applied potentials.

The diffusion coefficient and the nucleation rate as a function of the applied potential were calculated from Equations (4) and (5) and summarized in Table 3.

Table 3: Kinetic parameters resulting from Cu_2O deposited at different applied potentials.

E (V vs. SCE)	AN_0 ($cm^{-2}.s^{-1}$)	D_{prog} ($cm^2.s^{-1}$)
-0.4	$3.05\times10^{+5}$	1.18×10^{-7}
-0.5	$4.50\times10^{+5}$	1.41×10^{-7}
-0.6	$1.87\times10^{+6}$	2.18×10^{-7}

The results show that the diffusion coefficient of Cu^{2+} ions in the electrolyte increases from 1.18 to 2.18 × 10^{-7} $cm^2.s^{-1}$ when the applied potential increases from -0.4 to -0.6 V vs. SCE. In addition, the nucleation rate increases

to reach a maximum value of 1.87 × 10^{+6} cm^{-2}. s^{-1} at -0.6 V vs. SCE. This observation is due to the higher production of Cu^{+} and OH^{-} ions at the electrode/electrolyte interface at lower potentials [50].

3.2.2 Structural characterization

The structural characterizations of the electrodeposited Cu_2O nanostructures at different applied potentials are presented in Figure 7. XRD peaks of the electrodeposited Cu_2O films are assigned to the cubic phase with miller indices (110), (311), (200), (220), and (111) planes, respectively (JCPDS card N°: 01-078-2076) [51,52]. These peaks are narrow and sharp indicating that Cu_2O films presented a good crystalline, and their intensity increases as the deposition potential increases. Indeed, at -0.5 and -0.6 V vs. SCE, the peak intensity of (111) is more intense indicating the major growth of the Cu_2O thin films along the (111) direction [53,54].

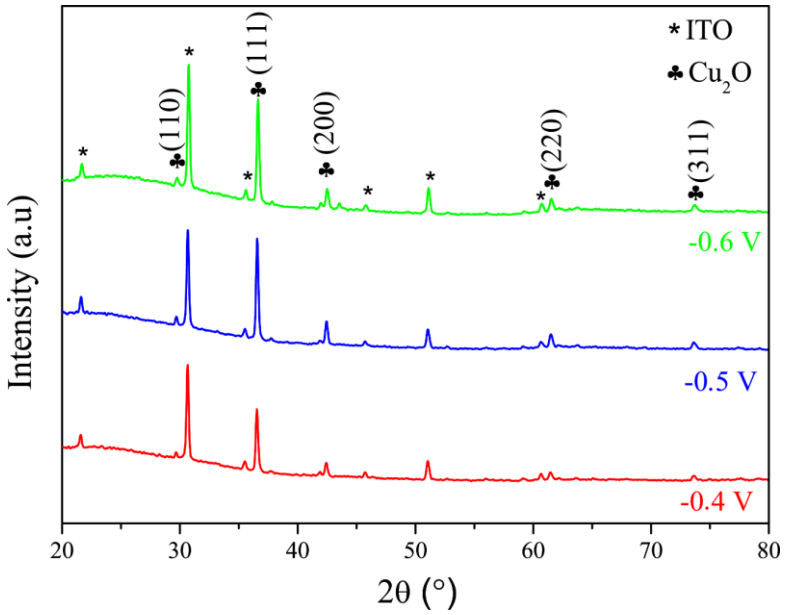

Figure 7: XRD patterns of Cu_2O nanostructures deposited at different applied potentials.

The crystallite sizes calculated from the (111) peak are 33.2, 31.2, and 30.7 nm for the potentials -0.4 V, -0.5 V, and -0.6 V, respectively. The same results were observed by Laidoudi et al. [55].

Table 4: The average crystallite size of Cu_2O estimated at (111) diffraction peak for different applied potentials.

E (V vs. SCE)	2θ (°)	D (nm)
-0.4	36.5	33.2
-0.5	36.6	31.2
-0.6	36.5	30.7

3.2.3 Morphological characterization

Figure 8 shows the SEM images of the electrodeposited Cu_2O films at different deposition potentials.

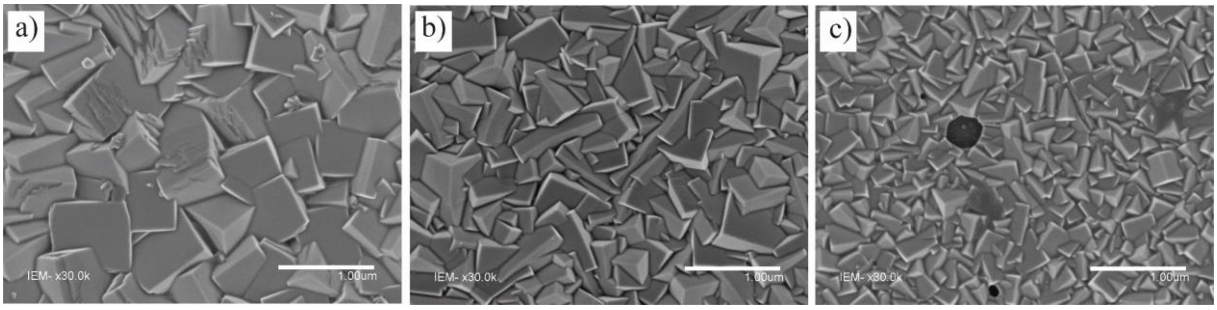

Figure 8: SEM images for Cu_2O films obtained at different applied potentials:

a) -0.4 V, **b)** -0.5 V, and **c)** -0.6 V vs. SCE.

The surface consisted of mixed large triangular prisms and cubic with sharp edges and corners, however, it is clear that the morphology changes with the employed potential. As deduced from XRD, the variation of the deposition potential influences the size of the crystallites through their influence on the growth kinetics. Nanostructures produced at a rapid nucleation rate are formed from small crystallites. Indeed, at a more negative potential, the deposition rate is high, which corresponds to a high mobility of atoms, which leads them to occupy as much as possible the voids. When a more negative potential is applied, the deposition rate increases, i.e. nucleation rate and growth process occur rapidly as well, so their rapid aggregation restricts their enlargement, resulting in a decrease in their size [50]. In contrast, when the Nucleation rate is slow, the nuclei have sufficient time to grow and form large grains. The results are consistent with those reported in the XRD section.

3.2.4 Optical characterization

Figure 9a shows the absorbance spectra for Cu_2O thin film grown at the different selected applied potentials. The materials show a strong absorption between 300 and 500 nm.

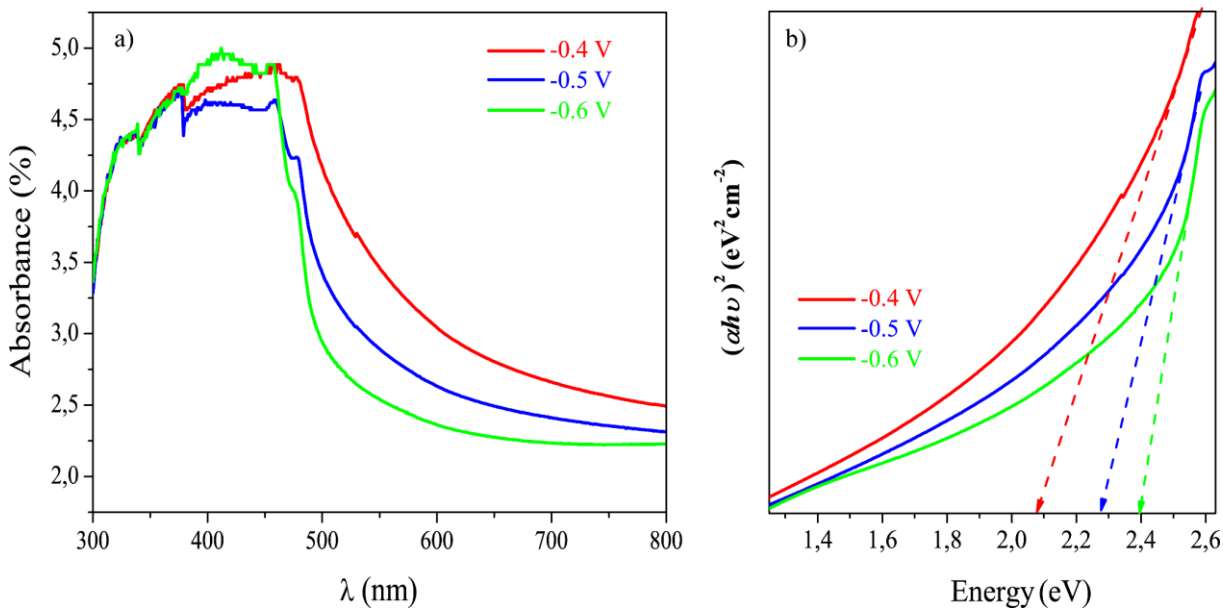

Figure 9: a) UV-vis spectral of Cu_2O grown at different selected applied potentials. **b)** Tauc plots for Cu_2O samples.

The band gaps of the developed Cu_2O thin films were estimated to be 2.09, 2.27, and 2.39 eV for -0.4, -0.5, and -0.6 V vs ECS, respectively, from the Tauc's plot shown in Figure 9b. As the potential increases towards negative values the absorption edge shifts toward shorter wavelengths indicating the widening of the optical gap of the film, caused by the small size of the crystallites [56,57]. Indeed, as we reported in Table 4, the size of crystallites dropped from 33.2 nm to 30.7 nm by increasing the deposition potential.

3.3 Effect of deposition time on the electrodeposition of Cu_2O

3.3.1 Structural characterization

Figure 10 depicts the structural state of Cu_2O films electrodeposited at -0.5 V vs. SCE for different deposition times ranging from 5 to 60 min. According to the JCPDS N°: 01-078-2076, all samples are mainly crystallized in the Cu_2O cubic phase, as indicated by their preference orientation along the (111) plane at $2\theta = 36.5°$. Furthermore, the XRD patterns clearly indicate the absence of secondary phases. The peak intensities were increased by increasing the deposition time from 5 to 60 min as shown in Table 5, indicating the structural improvement of Cu_2O films where the crystallinity increased as the deposition time increased.

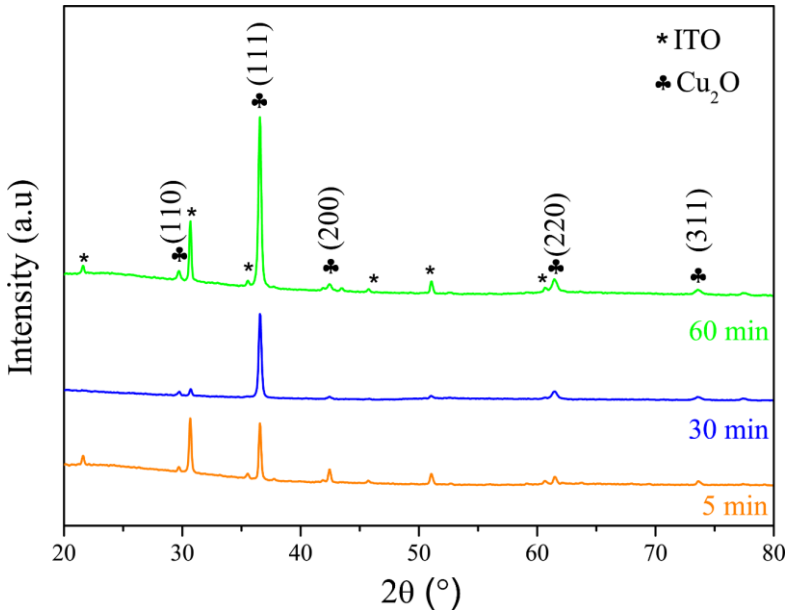

Figure 10: XRD patterns of Cu_2O nanostructures obtained at different deposition times.

The crystallite size calculated from (111) peak is 31.2, 32.1, and 42.3 nm for time 5, 30, and 60 min, respectively. The same results were observed by other authors [23,58–60].

Table 5: The average crystallite size of Cu_2O estimated at (111) diffraction peak for different deposition times.

Deposition time (min)	2θ (°)	D (nm)
5	36.5	31.2
30	36.5	32.1
60	36.5	42.3

3.3.2 Morphological characterization

The surface morphologies of the synthesized Cu_2O nanocrystals are revealed by SEM observations in Figure 11.

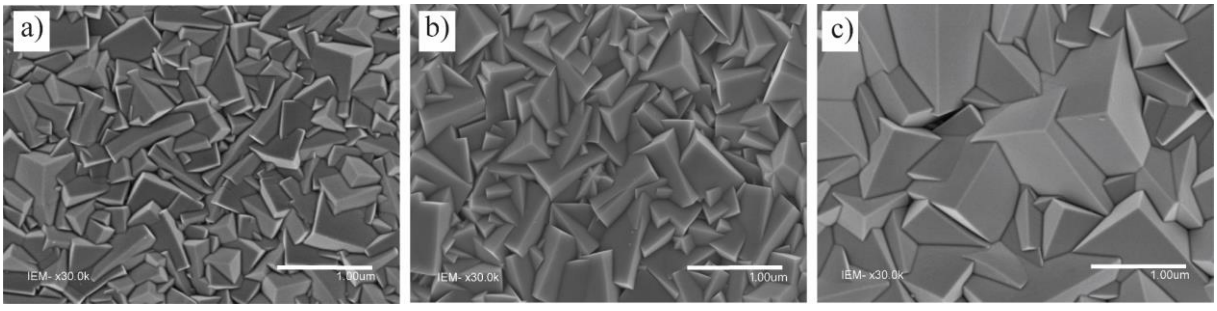

Figure 11: SEM images for Cu_2O films obtained at different deposition times: **a)** 5 min, **b)** 30 min, and **c)** 60 min.

It can be clearly observed in Figure 11 that the grain size and crystalline shape of the films are time-dependent [59]. The nanocrystal obtained at the shorter time (5 min) exhibited a mix of triangular prism and tetrahedron. By increasing the deposition time up to 30 min, the crystals become more compact, and their size increases. Increasing deposition time into 60 min big sized of tetrahedrons are observed. These results were consistent with XRD results where the deposition time influenced the morphology of the synthesized thin films.

3.3.3 Optical characterization

The absorbance spectra of Cu_2O thin films deposited on ITO glass synthesized at various deposition times are shown in Figure 12a. For all samples, the absorbance spectra show significant absorption in the visible range. Furthermore, a redshift was induced when the deposition time increased from 5 to 60 min. From Figure 12-b, the band gap (E_g) of the Cu_2O thin films decreased from 2.27, 2.23, and 2.17 eV as the deposition time increased from 5 to 60 min. In light of the previous XRD analysis, it can be deduced that the decrease in the optical band gap with increasing deposition time can be related to the improvement in crystallinity caused by the increase in crystallite size and the decrease in lattice strain during the deposition process [61]. Since the visible spectrum has a large portion of solar energy, a high absorbance in this region makes Cu_2O favorable as an absorber material.

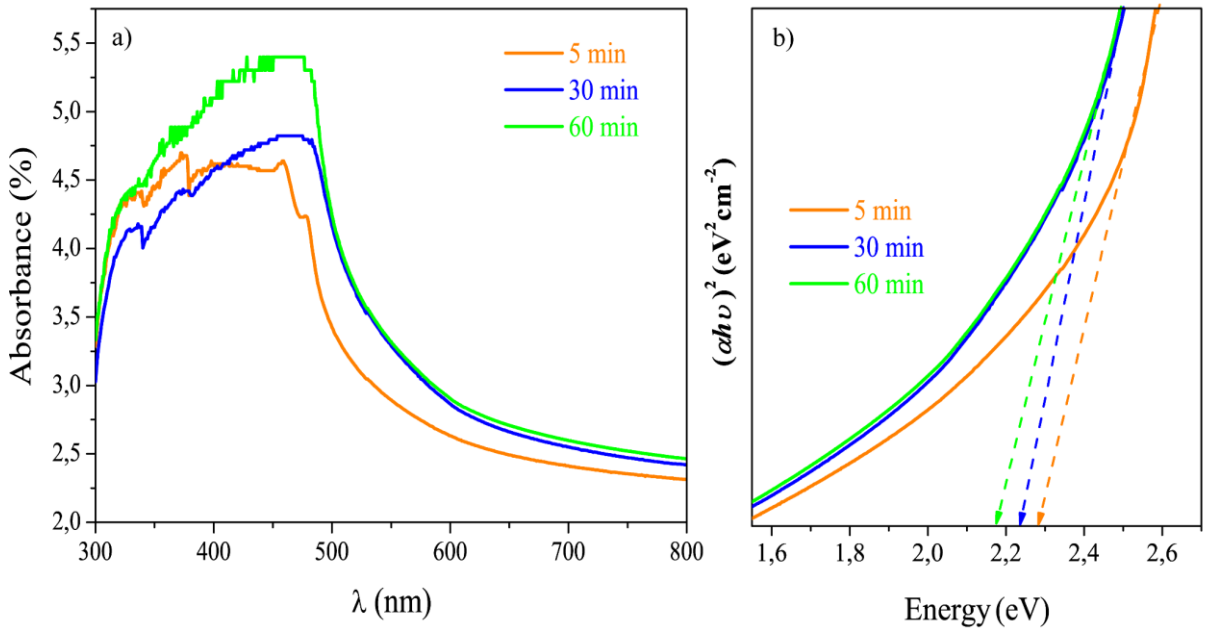

Figure 12: **a)** Absorption spectra of Cu_2O obtained at different deposition times. **b)** Tauc plots for Cu_2O samples calculated from the UV–visible data.

3.4 Test the synthesized Cu_2O thin films:

Cu_2O serves as the absorber layer in p-n heterojunction solar cells and hence is an essential component in the conversion of light into energy. The photocurrent measurement is a useful tool to give information about the electron-hole pairs' photo-generation and separation in a p-n heterojunction. In this section electrodeposited Cu_2O thin films under optimized conditions studied above (pH= 12.5, E= -0.5 V vs. SCE, and t= 60 min) were used as a p-type layer with ZnO as n-type layer to construct a p-n heterojunction. ZnO was used in two cases pure and doped with copper (Cu_2O/ZnO) and (Cu_2O/Cu-doped ZnO) [62]. Figure 13 represented the XRD, UV-Vis, and photocurrent measurement of the synthesized photoelectrode. Photoelectrochemical response under visible illumination was investigated using a halogen lamp (P= 250 w). The electrochemical cell contains the electrolyte in which the three electrodes used are immersed: working electrode (synthesized electrodes), counter electrode (Pt), and reference electrode (SCE).

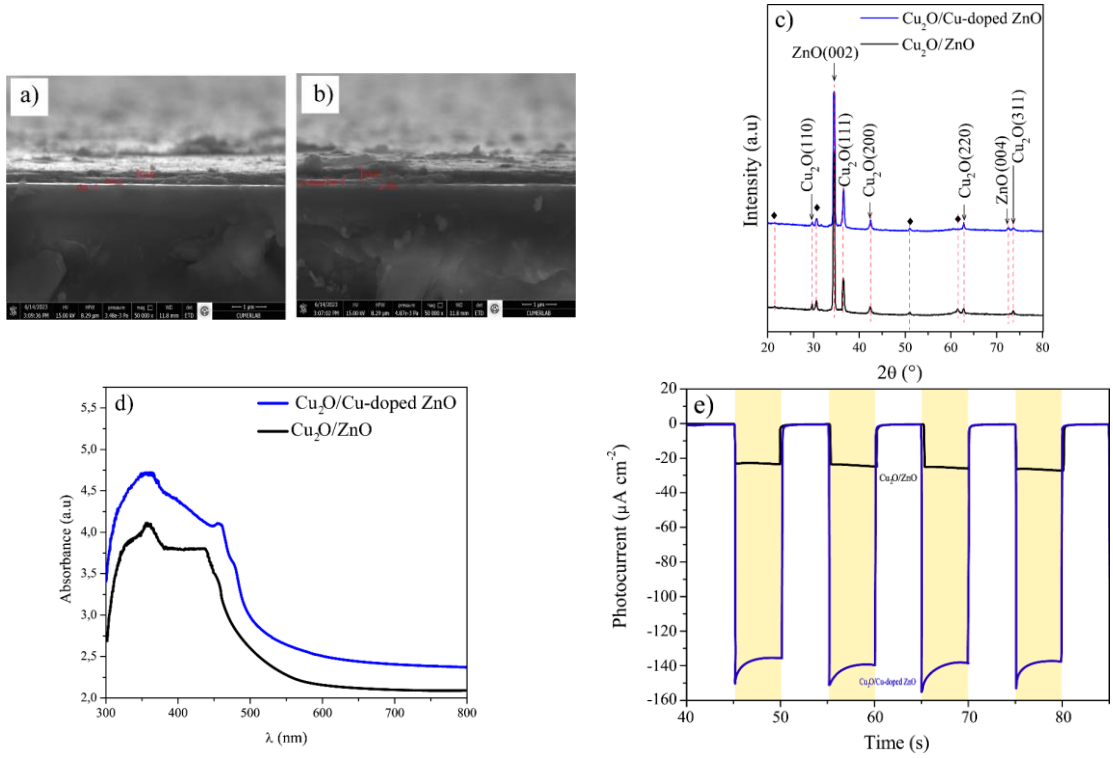

Figure 13: a) and b) cross section SEM images**, c)** XRD patterns, **d)** Absorption spectra, and **e)** photocurrent-time response of Cu_2O/ZnO and Cu_2O/Cu-doped ZnO thin films

As can be seen in Figure 13 (a and b), We distinguish three layers corresponding to ITO glass substrate, ZnO (or Cu-doped ZnO), and Cu_2O grown uniformly in the normal direction to the substrate surface. The crystalline structures are verified by the XRD spectrum shown in Figure 13b. The XRD patterns of both the Cu_2O/ZnO and Cu_2O/Cu-doped ZnO exhibit characteristic peaks corresponding to Cu_2O and ZnO thin films. Additionally, analysis of the absorbance spectra (Figure 13d) suggests that the synthesized Cu_2O/ZnO and Cu_2O/Cu-doped ZnO thin films can show good photoelectrochemical property under visible illumination due to reasonably broad absorption range, as confirmed by the last graph (Figure 13-c), where the photocurrent density was found to be 22 μA cm^{-2} for Cu_2O /ZnO photoelectrode, while this value increased dramatically to a maximum value of 140 μA cm^{-2} for Cu_2O /Cu-doped ZnO photoelectrode heterojunction. This improvement was more than 6 times more significant compared to pure ZnO. This fact demonstrated that the synthesized photoelectrode is shown to generate photoelectrochemical photocurrent and could be an efficient way to use as the best candidate for the generation of p-n heterojunction photoelectrochemical solar cells.

Conclusion

The main objective of this article is to study the electrochemical deposition of Cu_2O nanostructures on an ITO substrate and in parallel, to try to relate the effect of different parameters (pH, applied potential, and deposition time) on the electrochemical kinetic, morphological, optical, structural as well as the photoelectrical properties of the electrodeposited films.

It was found that the deposition of Cu_2O affected strongly with the pH of the bath solution where a high crystalline phase was obtained for a high pH (12.5), and by applying more negative potential. The deposition time revealed that the films obtained after 60 min exhibited high intensity of the predominant peak (111) and strong absorption in the range (400-500 nm).

The photocurrent measurements of Cu_2O coupled with Cu-doped ZnO suggested that the synthesized Cu_2O thin films with these conditions showed to be as a best candidate as a solar cell.

Declarations Conflict of interest

The authors declare there is no conflict of interest.

The authors declare that no funds, grants, or other support were received during the preparation of this manuscript

Data Availability

The data that support the findings of this study are available upon reasonable request.

References

[1] L.C.-K. Liau, C.-H. Tang, Effect of a Cu2O buffer layer on the efficiency in p-Cu2O/ZnO hetero-junction photovoltaics using electrochemical deposition processing, J Appl Electrochem 52 (2022) 1459–1467.

[2] G.C. Enebe, V.T. Lukong, R.T. Mouchou, K.O. Ukoba, T.C. Jen, Optimizing nanostructured TiO2/Cu2O pn heterojunction solar cells using SCAPS for fourth industrial revolution, Mater Today Proc 62 (2022) S145–S150.

[3] S.I. Kunya, Y. Abdu, M.K. Mustafa, M.K. Ahmad, Cuprous Oxide (Cu2O) Based Solar Cell Thickness Dependence, British Journal of Physics Studies 1 (2022) 1–7.

[4] Y. Wang, C.K.G. Kwok, D. Xiao, J. Zhu, X. Shu, C.P. Liu, K.M. Yu, Improving the p–type conductivity of Cu2O thin films by Ni doping and their heterojunction with n–ZnO, Appl Surf Sci 590 (2022) 153047.

[5] S. Derbal, M. Benaicha, Insights on the Effect of Applied Potential on the Properties of Electrodeposited p-Type Cuprous Oxide (Cu2O) Thin Films, J Electron Mater 50 (2021) 5134–5140.

[6] F. Fenniche, A. Henni, Y. Khane, D. Aouf, N. Harfouche, S. Bensalem, D. Zerrouki, H. Belkhalfa, Electrochemical Synthesis of Reduced Graphene Oxide–Wrapped Polyaniline Nanorods for Improved Photocatalytic and Antibacterial Activities, J Inorg Organomet Polym Mater (2022) 1–15.

[7] S. Islam, M.M. Mia, S.S. Shah, S. Naher, M.N. Shaikh, M.A. Aziz, A.J.S. Ahammad, Recent Advancements in Electrochemical Deposition of Metal-Based Electrode Materials for Electrochemical Supercapacitors, The Chemical Record 22 (2022) e202200013.

[8] D. Aouf, A. Henni, D. Selloum, Y. Khane, F. Fenniche, D. Zerrouki, H. Belkhalfa, N. Dizge, Facile preparation and characterization of nanostructured ZnS/PbS heterojunction thin films for enhanced microbial inhibition and photocatalytic degradation, Mater Chem Phys 295 (2023) 127059.

[9] F.Z. Nouasria, D. Selloum, A. Henni, S. Tingry, J. Hrbac, Improvement of the photocatalytic performance of ZnO thin films in the UV and sunlight range by Cu doping and additional coupling with Cu2O, Ceram Int 48 (2022) 13283–13294.

[10] A. Boulett, G.D.C. Pizarro, R. Martin-Trasanco, J. Sánchez, F. Tasca, O.E. Linarez Pérez, A. Tello, D.P. Oyarzún, Electrodeposition of Cu2O nanostructures with improved semiconductor properties, Cogent Eng 8 (2021) 1875534.

[11] H. Rahal, R. Kihal, A.M. Affoune, S. Rahal, Effect of Solution pH on Properties of Cuprous Oxide Thin Films Prepared by Electrodeposition from a New Bath, J Electron Mater 49 (2020) 4385–4391.

[12] Y. Yang, M. Pritzker, Y. Li, Electrodeposited p-type Cu2O thin films at high pH for all-oxide solar cells with improved performance, Thin Solid Films 676 (2019) 42–53.

[13] C. Ravichandiran, A. Sakthivelu, R. Davidprabu, S. Valanarasu, A. Kathalingam, V. Ganesh, M. Shkir, H. Algarni, S. AlFaify, In-depth study on structural, optical, photoluminescence and electrical properties of electrodeposited Cu2O thin films for optoelectronics: An effect of solution pH, Microelectron Eng 210 (2019) 27–34.

[14] I.R. Hamdani, A.N. Bhaskarwar, Tuning of the structural, morphological, optoelectronic and interfacial properties of electrodeposited Cu2O towards solar water-splitting by varying the deposition pH, Solar Energy Materials and Solar Cells 240 (2022) 111719.

[15] J. Bahar, Y. Lghazi, B. Youbi, M.A. Himi, C. El Haimer, A. Ouedrhiri, A. Aynaou, I. Bimaghra, Nucleation and growth mechanism of cuprous oxide electrodeposited on ITO substrate, Mater Today Proc 66 (2022) 187–195.

[16] S. Derbal, M. Benaicha, Insights on the Effect of Applied Potential on the Properties of Electrodeposited p-Type Cuprous Oxide (Cu2O) Thin Films, J Electron Mater 50 (2021) 5134–5140.

[17] A. Maddu, Influence of Applied Potential on The Structural and Optical Properties of Cu2O Thin Films Grown by Electrochemical Deposition, Jurnal Sains Materi Indonesia 24 (2022) 16–23.

[18] S.J. Taher, A.A. Barzinjy, S.M. Hamad, The Effect of Deposition Time on the Properties of Cu2O Nanocubes Using an Electrochemical Deposition Method, J Electron Mater 49 (2020) 7532–7540.

[19] A.A. Hssi, L. Atourki, N. Labchir, M. Ouafi, K. Abouabassi, A. Elfanaoui, A. Ihlal, K. Bouabid, Optical and dielectric properties of electrochemically deposited p-Cu2O films, Mater Res Express 7 (2020) 16424.

[20] S. Laidoudi, M.R. Khelladi, C. Dehchar, S. Boudour, L. Lamiri, O. Belgherbi, R. Boufnik, Optical, structural and morphological characterization of electrodeposited cuprous oxide thin films: Effect of deposition time, 5th International Conference On Advances In Mechanical Engineering (2019) 1–14.

[21] F. Tezcan, A. Mahmood, G. Kardaş, The investigation of Cu2O electrochemical deposition time effect on ZnO for water splitting, J Mol Struct 1193 (2019) 342–347.

[22] N.M. Rosas-Laverde, A. Pruna, J. Cembrero, J. Orozco-Messana, F.J. Manjón, Performance of graphene oxide-modified electrodeposited ZnO/Cu2O heterojunction solar cells, Boletin de La Sociedad Espanola de Ceramica y Vidrio 58 (2019) 263–273.

[23] S. Laidoudi, M.R. Khelladi, C. Dehchar, S. Boudour, L. Lamiri, O. Belgherbi, R. Boufnik, Optical, structural and morphological characterization of electrodeposited cuprous oxide thin films: Effect of deposition time, 5th International Conference On Advances In Mechanical Engineering (2019) 1–14.

[24] R. Kara, S. Rachid, A. Azizi, Effect of i-ZnO seed layer on the properties of electrodeposited p-Cu2O/n-ZnO/FTO heterojunction thin films, Mater Res Express 6 (2019) 126402.

[25] M.A. Hossain, R. Al-Gaashani, H. Hamoudi, M.J. Al Marri, I.A. Hussein, A. Belaidi, B.A. Merzougui, F.H. Alharbi, N. Tabet, Controlled growth of Cu2O thin films by electrodeposition approach, Mater Sci Semicond Process 63 (2017) 203–211.

[26] Z. Grzesik, M. Migdalska, Oxidation mechanism of Cu2O and defect structure of CuO at high temperatures, High Temperature Materials and Processes 30 (2011) 277–287.

[27] J.T. Matsushima, L.C.D. Santos, A.B. Couto, M.R. Baldan, N.G. Ferreira, Electrodeposition of Cu Nanoparticles on BDD Electrodes: Reactions and Nucleation Mechanism, J Electrochem Soc 159 (2012) D246–D252.

[28] M.M. Moharam, E.M. Elsayed, J.C. Nino, R.M. Abou-Shahba, M.M. Rashad, Potentiostatic deposition of Cu2O films as p-type transparent conductors at room temperature, Thin Solid Films 616 (2016) 760–766.

[29] A.A. Hssi, L. Atourki, K. Abouabassi, A. Elfanaoui, K. Bouabid, A. Ihlal, S. Benmokhtar, M. Ouafi, Growth and characterization of Cu2O for solar cells applications, AIP Conf Proc 2056 (2018) 2–8.

[30] X. Yu, X. Tang, J. Li, J. Zhang, S. Kou, J. Zhao, B. Yao, Nucleation Mechanism and Optoelectronic Properties of Cu 2 O onto ITO Electrode in the Electrochemical Deposition Process, J Electrochem Soc 164 (2017) D999–D1005.

[31] M.M. Moharam, E.M. Elsayed, J.C. Nino, R.M. Abou-Shahba, M.M. Rashad, Potentiostatic deposition of Cu2O films as p-type transparent conductors at room temperature, Thin Solid Films 616 (2016) 760–766.

[32] Y. Yang, Y. Li, M. Pritzker, Control of Cu2O Film Morphology Using Potentiostatic Pulsed Electrodeposition, Electrochim Acta 213 (2016) 225–235.

[33] P. Wang, Y.H. Ng, R. Amal, Embedment of anodized p-type Cu2O thin films with CuO nanowires for improvement in photoelectrochemical stability, Nanoscale 5 (2013) 2952–2958.

[34] F. Chaffar Akkari, H. Ben Jbara, D. Abdelkader, B. Gallas, M. Kanzari, Effect of angle deposition γ on the structural, optical and electrical properties of copper oxide zigzag (+γ, −γ) nanostructures elaborated by glancing angle deposition, Thin Solid Films 657 (2018) 61–69.

[35] Q.B. Ma, J.P. Hofmann, A. Litke, E.J.M. Hensen, Cu2O photoelectrodes for solar water splitting: Tuning photoelectrochemical performance by controlled faceting, Solar Energy Materials and Solar Cells 141 (2015) 178–186. https://doi.org/10.1016/j.solmat.2015.05.025.

[36] H. Rahal, R. Kihal, A.M. Affoune, S. Rahal, Effect of Solution pH on Properties of Cuprous Oxide Thin Films Prepared by Electrodeposition from a New Bath, J Electron Mater 49 (2020) 4385–4391.

[37] Y. Yang, M. Pritzker, Y. Li, Electrodeposited p-type Cu2O thin films at high pH for all-oxide solar cells with improved performance, Thin Solid Films 676 (2019) 42–53.

[38] I.S. Brandt, C.A. Martins, V.C. Zoldan, A.D.C. Viegas, J.H.D. da Silva, A.A. Pasa, Structural and optical properties of Cu2O crystalline electrodeposited films, Thin Solid Films 562 (2014) 144–151.

[39] L.C. Wang, N.R. de Tacconi, C.R. Chenthamarakshan, K. Rajeshwar, M. Tao, Electrodeposited copper oxide films: Effect of bath pH on grain orientation and orientation-dependent interfacial behavior, Thin Solid Films 515 (2007) 3090–3095.

[40] Y. Zhou, J.A. Switzer, Electrochemical deposition and microstructure of copper (I) oxide films, Scr Mater 38 (1998) 1731–1738.

[41] P.K. Pagare, A.P. Torane, Electrodeposition and characterization of pH transformed Cu2O thin films for electrochemical sensor, Journal of Materials Science: Materials in Electronics 28 (2017) 1386–1392.

[42] Q.B. Ma, J.P. Hofmann, A. Litke, E.J.M. Hensen, Cu2O photoelectrodes for solar water splitting: Tuning photoelectrochemical performance by controlled faceting, Solar Energy Materials and Solar Cells 141 (2015) 178–186. https://doi.org/10.1016/j.solmat.2015.05.025.

[43] L.C. Wang, N.R. de Tacconi, C.R. Chenthamarakshan, K. Rajeshwar, M. Tao, Electrodeposited copper oxide films: Effect of bath pH on grain orientation and orientation-dependent interfacial behavior, Thin Solid Films 515 (2007) 3090–3095.

[44] P.K. Pagare, A.P. Torane, Electrodeposition and characterization of pH transformed Cu2O thin films for electrochemical sensor, Journal of Materials Science: Materials in Electronics 28 (2017) 1386–1392.

[45] C. Wang, J. Xu, S. Shi, Y. Zhang, Z. Liu, X. Zhang, S. Yin, L. Li, Structural, optical and photoelectrical properties of Cu2O films electrodeposited at different pH, RSC Adv 6 (2016) 4422–4428.

[46] C. Ravichandiran, A. Sakthivelu, R. Davidprabu, S. Valanarasu, A. Kathalingam, V. Ganesh, M. Shkir, H. Algarni, S. AlFaify, In-depth study on structural, optical, photoluminescence and electrical properties of electrodeposited Cu2O thin films for optoelectronics: An effect of solution pH, Microelectron Eng 210 (2019) 27–34.

[47] S. Bijani, R. Schrebler, E.A. Dalchiele, M. Gabás, L. Martínez, J.R. Ramos-Barrado, Study of the nucleation and growth mechanisms in the electrodeposition of micro- and nanostructured Cu2O thin films, Journal of Physical Chemistry C 115 (2011) 21373–21382.

[48] S. Bijani, L. Martínez, M. Gabás, E.A. Dalchiele, J.R. Ramos-Barrado, Low-temperature electrodeposition of Cu2O thin films: Modulation of micro-nanostructure by modifying the applied potential and electrolytic bath pH, Journal of Physical Chemistry C 113 (2009) 19482–19487.

[49] D.G. Mohan, S. Gopi, V. Rajasekar, K. Krishnan, D.G. Mohan, Gopi S., L. Selvarajan, R. Rajavel, B. Prakash, D.G. Mohan, S. Gopi, A.A. Alloys, U. Taguchi, L. Selvarajan, R. Sasikumar, D.G. Mohan, P. Naveen Kumar, V. Muralidharan, Optical and dielectric properties of electrochemically deposited p-Cu2O films, Mater Today Proc 27 (2019) 0–31.

[50] S. Bijani, R. Schrebler, E.A. Dalchiele, M. Gabás, L. Martínez, J.R. Ramos-Barrado, Study of the nucleation and growth mechanisms in the electrodeposition of micro- and nanostructured Cu2O thin films, Journal of Physical Chemistry C 115 (2011) 21373–21382.

[51] P. Wang, Y.H. Ng, R. Amal, Embedment of anodized p-type Cu2O thin films with CuO nanowires for improvement in photoelectrochemical stability, Nanoscale 5 (2013) 2952–2958.

[52] F. Chaffar Akkari, H. Ben Jbara, D. Abdelkader, B. Gallas, M. Kanzari, Effect of angle deposition γ on the structural, optical and electrical properties of copper oxide zigzag (+γ, −γ) nanostructures elaborated by glancing angle deposition, Thin Solid Films 657 (2018) 61–69.

[53] S. Laidoudi, A.Y. Bioud, A. Azizi, G. Schmerber, J. Bartringer, S. Barre, A. Dinia, Growth and characterization of electrodeposited Cu2O thin films, Semicond Sci Technol 28 (2013) 115005.

[54] A. Ait Hssi, L. Atourki, N. Labchir, M. Ouafi, K. Abouabassi, A. Elfanaoui, A. Ihlal, S. Benmokhtar, K. Bouabid, High-quality Cu2O thin films via electrochemical synthesis under a variable applied potential, Journal of Materials Science: Materials in Electronics 31 (2020) 4237–4244.

[55] S. Laidoudi, A.Y. Bioud, A. Azizi, G. Schmerber, J. Bartringer, S. Barre, A. Dinia, Growth and characterization of electrodeposited Cu2O thin films, Semicond Sci Technol 28 (2013) 115005.

[56] F. Hu, K.C. Chan, T.M. Yue, C. Surya, Electrochemical synthesis of transparent nanocrystalline Cu2O films using a reverse potential waveform, Thin Solid Films 550 (2014) 17–21.

[57] Y. Zhai, H. Fan, Q. Li, W. Yan, Morphology evolutions and optical properties of Cu 2 O films by an electrochemical deposition on flexible substrate, Appl Surf Sci 258 (2012) 3232–3236.

[58] O. Messaoudi, I. Ben Assaker, M. Gannouni, A. Souissi, H. Makhlouf, A. Bardaoui, R. Chtourou, Structural, morphological and electrical characteristics of electrodeposited Cu 2 O: Effect of deposition time, Appl Surf Sci 366 (2016) 383–388.

[59] A.A. Hssi, L. Atourki, N. Labchir, M. Ouafi, K. Abouabassi, A. Elfanaoui, A. Ihlal, K. Bouabid, Optical and dielectric properties of electrochemically deposited p-Cu2O films, Mater Res Express 7 (2020) 16424.

[60] A.S. Mohd Hanif, S.A. Azmal, M.K. bin Ahmad, F. Mohamad, Effect of deposition time on the electrodeposited n-Cu2O thin film, Applied Mechanics and Materials 773 (2015) 677–681.

[61] O. Messaoudi, I. Ben Assaker, M. Gannouni, A. Souissi, H. Makhlouf, A. Bardaoui, R. Chtourou, Structural, morphological and electrical characteristics of electrodeposited Cu 2 O: Effect of deposition time, Appl Surf Sci 366 (2016) 383–388.

[62] F.Z. Nouasria, D. Selloum, A. Henni, D. Zerrouki, S. Tingry, Gradient doping of Cu(I) and Cu(II) in ZnO nanorod photoanode by electrochemical deposition for enhanced photocurrent generation, Ceram Int 47 (2021) 19743–19751.